Comparison of surface extraction techniques performance in computed tomography for 3D complex micro-geometry dimensional measurements

Marta Torralba [1], Roberto Jiménez [1], José A. Yagüe-Fabra [2,*], Sinué Ontiveros [3], Guido Tosello [4]

[1] Centro Universitario de la Defensa, A.G.M. Carretera Huesca s/n, 50090 Zaragoza; martatg@unizar.es; rjimenez@unizar.es

[2] I3A, Universidad de Zaragoza, María de Luna 3, 50018 Zaragoza; jyague@unizar.es; ORCID: 0000-0001-7152-4117

[3] Department of Industrial Engineering, Autonomous University of Baja California, Mexico; sinue.ontiveros@uabc.edu.mx

[4] Department of Mechanical Engineering, Technical University of Denmark, Kgs. Lyngby, Denmark; guto@mek.dtu.dk

* Correspondence: jyague@unizar.es; Tel.: +34-976-762-561

Abstract: The number of industrial applications of Computed Tomography (CT) for dimensional metrology in 10^0-10^3 mm range has been continuously increasing, especially in the last years. Due to its specific characteristics Computed Tomography has the potential to be employed as a viable solution for measuring 3D complex micro-geometries as well (i.e. in the sub-mm dimensional range). However, there are different factors that may influence the CT process performance, being one of them the surface extraction technique used. In this paper two different extraction techniques are applied to measure a complex miniaturized dental file by CT in order to analyze its contribution to the final measurement uncertainty in complex geometries at the mm to sub-mm scales. The first method is based on a similarity analysis: the threshold determination; while the second one is based on a gradient or discontinuity analysis: the 3D Canny algorithm. This algorithm has proven to provide accurate results in parts with simple geometries, but its suitability for 3D complex geometries has not been proven so far. To verify the measurement results and compare both techniques, reference measurements are performed on an optical coordinate measuring machine (OCMM). The systematic errors and uncertainty results obtained show that the 3D Canny adapted method slightly lower systematic deviations and a more robust edge definition than the local threshold method for 3D complex micro-geometry dimensional measurements.

Keywords: 3D complex geometry; Computed Tomography; Surface extraction; Canny algorithm

1. Introduction

The geometrical complexity of industrial components with micro three-dimensional features has been rapidly increasing in the last years. That implies a parallel effort from the metrology point of view in order to assure the correct dimensional measurement and tolerance verification of these parts [1]. Tactile and optical techniques are available to perform length measurements in three dimensions with high accuracy. However, they exhibit limitations when measuring 3D complex geometries, especially at sub-mm scale [2–4]. Tactile techniques are limited in terms of accessibility and minimum measurable feature size due to the probe and stylus dimensions, measuring point density and deformation of high aspect ratio structures under measurement and of soft substrate materials due to the probing force. Non-contact techniques, such as interferometric microscopes [5] or laser line scanning [6] have limitations both in measuring vertical walls and high aspect ratio structures, due to surface properties and accessing out-of-sight features. In recent years, 3D imaging by means of Computed Tomography (CT) has emerged as a new technology for industrial quality control in many industrial applications [7]. The main metrological capability of this non-contact

47 imaging technique is based on the possibility of acquiring a densely populated 3D scanning point
48 cloud of an object, allowing the measuring of free-form surfaces [8], non-accessible internal
49 structures [9,10] and even multi-material components [11–13]. Therefore, regarding 3D complex
50 surface geometries, Computed Tomography has the potential to become a viable solution for their
51 dimensional measuring. However, CT metrology improvements have been initially focused on the
52 measurement of reference standards and industrial parts that are characterized by simple or regular
53 geometries, i.e. intrinsically linear or approximated by linear forms (lines, planes, circles, spheres,
54 cylinders, etc.) [14–16] and the study and optimization of this technique for 3D complex
55 micro-geometry dimensional measurements has not been addressed so far.

56   The main disadvantage of CT is the high number and the complexity of the factors related to
57 hardware, software, environment, workpiece and operator that may influence the system
58 performance [17–19]. Previous works [17–19] have already addressed the difficulty of identifying
59 and quantifying all the uncertainty sources that should be considered for a measurement uncertainty
60 evaluation. In addition, research has been carried out to demonstrate and evaluate the contribution
61 of specific factors with regards to metrology issues: for instance, the work presented in [20] is
62 focused on those influencing factors that can be controlled by the machine operator (e.g.
63 magnification of the workpiece, number of projections, position and orientation of the workpiece).
64 Simulated computed tomography data is used in [21] to investigate the effect of angular
65 misalignments of a flat-panel detector, and in [22] for studying the influence factors on image quality
66 and scanning geometry by numerical generation modelling of X-ray projections. A more extensive
67 review of geometrical influence factors is outlined by Ferrucci et al. in [23] with respect to the
68 geometrical offsets and misalignments of the cone-beam CT system. Hiller et al. compared the
69 results when measuring a test object with two CT systems, two STL models provided by each of the
70 scanners and two different software packages for geometrical fitting [24]. Different measuring
71 strategies are also compared in [25], where three different inspection software packages for volume
72 and surface data analysis were applied. Additionally, the authors in [26] evaluated and quantified
73 the repeatability of post-processing settings, such as data fitting, the definition of the datum system
74 and surface determination, which is also analyzed in [27,28]. As some of these works show, the
75 surface extraction technique used is one of the most influent factors in the final measurement
76 uncertainty.

77   All these studies have been also carried out using parts with simplified geometrical shapes to be
78 analyzed. However, when the influences of these factors are to be studied on 3D free-form
79 geometries or complex shapes, and particularly when they belong to micro-components, their
80 evaluation becomes more complicated. The direct comparison between calibrated values and
81 measured values of 3D complex geometries is more challenging than for, for example, spheres,
82 cylinders, etc. The goal of the present work is to study the influence of two different surface
83 extraction techniques in the final systematic error and measurement uncertainty when applied to
84 measure a complex miniaturized component for medical applications (dental endodontic file) by CT.
85 The first method is based on the threshold determination strategy [29,30], widely used in
86 commercial CT systems and based on the similarity principle. The second one is based on a
87 discontinuity analysis by applying the 3D Canny adapted algorithm developed by the authors in
88 [31]. Both methods have been previously studied by the authors in order to, firstly, analyze
89 advantages and drawbacks of using CT metrology in comparison with other measuring systems in
90 micro-molded parts with regular geometries [29] and, secondly, carry out a mutual comparison of
91 both surface extraction techniques applied to parts or reference standards also with regular
92 geometries [30-32]. In all these previous works reference calibration objects with regular geometries
93 were used. The same types of reference objects with regular geometries are found in the literature
94 published for other authors [23-27]. In the present work the authors propose a real object with
95 complex 3D geometry, which is an innovation with respect to the previous works found in the
96 literature. This presents some challenges, especially for the 3D Canny algorithm since, as described
97 in [31] it uses an strategy that analyses the surface from the three main Cartesian directions in order
98 to extract the surface. That was proven to be effective with regular surfaces than can be easily

99 defined along those Cartesian axes [31]. However, in 3D complex geometries, which are not
100 necessarily aligned with those Cartesian axes, the effectiveness of these algorithms has to be
101 analyzed, what becomes the main objective and novelty of the present work.

102 To verify the CT measurement results and compare both methods, the dental file is also
103 characterized by an optical CMM (OCMM). Hence, the paper is organized as follows. Firstly, Section
104 2 introduces the workpiece and workflow applied in dimensional CT metrology, the description of
105 the surface extraction methods and the common measurement strategy considered for the OCMM
106 and the CT systems. In Section 3, the measurement results are presented. The systematic error
107 analysis and the uncertainty estimation for both OCMM and CT measurements are included, also
108 describing the assessment of the CT system tolerance verification capability in order to compare the
109 results of both surface extraction techniques. The article ends in Section 4 with the conclusions about
110 the strong points and weaknesses of both techniques when they are applied to the geometrical
111 measurement of 3D complex shapes of micro-components.

112 **2. Materials and Methods**

113 *2.1. Workpiece: 3D complex geometry dental file*

114 A complex miniaturized component for medical applications, a dental file [33,34], was
115 considered for this study. The ProTaper F2 finishing file (produced by Dentsply Maillefer, York, PA,
116 USA) is made of Nickel Titanium (Ni-Ti) alloy and presents complex helix geometry, due to its
117 variable sub-mm diameter, and variable helix pitch and helix angle along its axis. Figure 1 shows a
118 detail of the active cutting part of the file. Its measurands are defined according to ISO 3630-1:2008
119 [35], being the following (see Figure 2):

120 • Length of the active cutting part (**La**).
121 • Variable diameter along the file length (**Dn**, n=0,1,2,…,12).
122 • Helix angle (**Hn**, n=1,…,9) or the angle formed between the helix and the file axial axis.
123 • Helix pitch (**Pn**, n=1,…,9) or the distance between a point in the forward edge and its
124 corresponding point in the adjacent edge along the file longitudinal axis.

125 The diameter Dr is used as a reference value for the surface extraction techniques since it can be
126 easily calibrated by tactile methods. The standard [35] specifies nominal values for the cutting
127 segment (La, 16 mm length); tip diameter (D0, 0.25 mm); fixed conicity (8% between D0 and D3);
128 variable conicity from D3 to D12 along its axis; and a maximal flute diameter (Dr, 1.20 mm). Other
129 dimensional features are specified neither by the standards, nor by the manufacturer, so that the
130 tolerances used in this work are based only on the previously mentioned. For diameters from D0 to
131 D6, their tolerance is ±20 μm. For diameters from D7 to D12, the specified tolerance is ±40 μm. For
132 the active cutting length (La) the tolerance is ±0.5 mm.

133

134 **Figure 1.** Dental file workpiece: detailed view of the active cutting part with complex helix geometry
135 and variable sub-mm diameter. Image obtained from the OCMM.
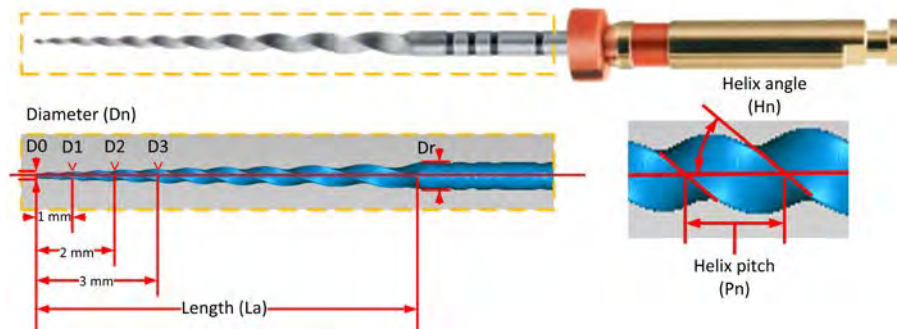
Figure 2. Dental file workpiece: characteristic dimensions to be verified by computed tomography La (length), Dn (diameter), Pn (helix pitch) and Hn (helix angle).

2.2. Dimensional CT metrology workflow

As mentioned before, the metrological capability of CT systems is limited by the numerous and complex factors which influence the system performance. In the literature, the measurement error sources have been classified by different criteria [18,19]. In brief, the main factors are the following:

- CT-system or hardware (X-ray source, rotary table, detector, global CT-scan geometry, etc.).
- Software and data processing (reconstruction algorithm, surface detection methods, data correction, etc.).
- Environment (temperature, humidity, vibrations, etc.).
- Workpiece (geometry, material, manufacturing variations, surface roughness, etc.).
- Operator (scanning parameters, experience, etc.).

These influencing factors are present in the different required steps in CT measurements. These phases and the typical process chain of dimensional measurement by means of CT are schematized in Figure 3. First, the 2D X-ray scans provide the projected images of the measured workpiece. Secondly, the images are reconstructed into a 3D voxel model. Then, the segmentation phase allows distinguishing the edges from the point cloud of the workpiece by using surface extraction algorithms. To conclude, dimensions of measurands are determined by a fitting procedure. It is after this final phase when the evaluation of the results can be carried out, including the measurement uncertainty estimation. In this work, the different parameters of the dental file were measured both by the CT scanner and, previously, by an optical coordinate measuring machine (OCMM) as a reference in order to be able to carry out a result comparison with a calibrated measuring system.

Recent research demonstrates that the measurement uncertainty value is mainly affected by both the post-processing strategy and the user influence [36]. Thus, the post-processing phase can be considered one of the key phases in terms of uncertainty evaluation. Therefore, two surface extraction techniques are applied in this work in order to compare them by analyzing the results obtained when measuring a miniaturized dental file having a 3D complex geometry. Both methods briefly described later are the following: CT1 or local threshold method [29] and CT2 based on the 3D Canny algorithm [31].
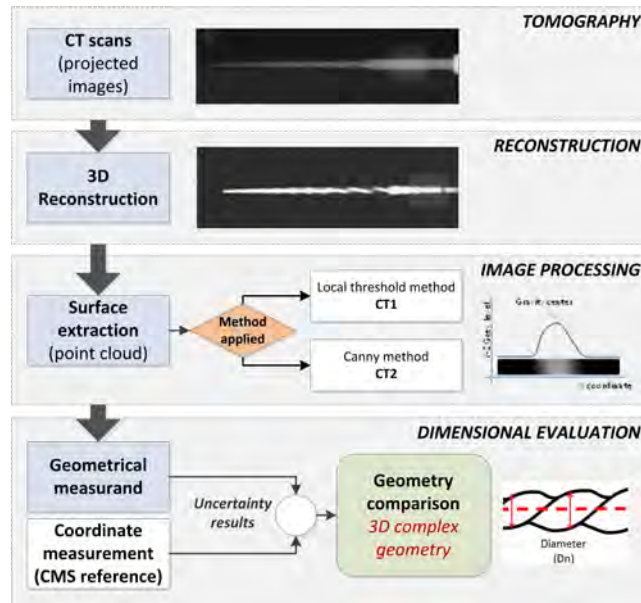
Figure 3. Workflow or process chain for CT measurement evaluation: case study of a miniaturized dental file with 3D complex geometry.

2.3. Surface extraction techniques applied: Local threshold and 3D Canny algorithm

Two different techniques were applied for the surface extraction to perform the measurements of the workpiece by computed tomography: CT1 or local threshold method [29] and CT2 based on the 3D Canny algorithm [31]. Both techniques have been already applied to common geometric primitives (basic geometric shapes and forms, e.g. lines, planes, spheres…). In this work, where they are applied to complex geometries, the point clouds obtained by each technique are processed using the same measurement protocol with Metrolog XG software by Metrologic Group (Meylan, France). The brief description of both techniques is included below.

2.3.1. Local threshold method (CT1)

The specific CT1 technique used in this case needs a correction by locally adapting the threshold value, as explained later. Threshold method for surface extraction in CT is a well-known technique adapted from the 2D image segmentation. It is based on the determination of a gray value (called threshold) used to distinguish one material to the other. Voxels with higher gray value than threshold are considered belonging to the part, and voxels with lower value are considered as air. After that, sub-voxel techniques based on a local 3D interpolation are used to determinate the surface points.
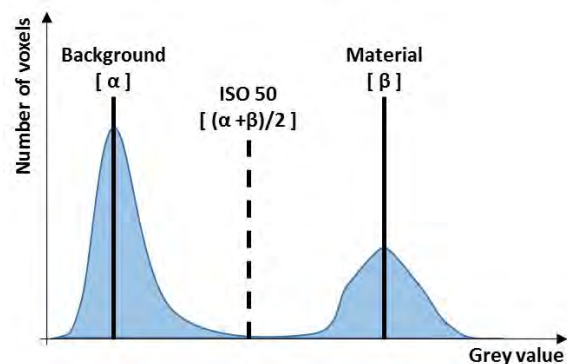
Figure 4. Determination of the threshold value based on the ISO50 method.

Threshold value can be determined using the ISO50 method [37]. This method is based on the determination of a reference gray value for each of the two materials, and the calculation of the

189 ISO50 threshold value as their average. The reference value for each material is usually calculated as
190 the peak value assigned to that material in the histogram graph (Figure 4). Although this method is
191 widely used in multiple applications due to its simplicity, it does not guarantee an accurate
192 determination of the surface [22,28]. Therefore, in this work, the threshold value obtained by the
193 ISO50 method has been corrected. The correction method is based on finding, by an iterative
194 process, a threshold value which minimizes the deviation between the reference value for Dr
195 (obtained by an additional and more accurate tactile coordinate measuring system, a CMM with
196 $MPE_{CMM} = 2.3$ μm + (L/300) μm, L in mm) and the measured value for Dr (see Caption Figure 2). A
197 more detailed explanation of the whole process can be found in [29].

198 2.3.2. Canny algorithm (CT2)

199 Developed by the authors and implemented using the Matlab software by MathWorks (Natick,
200 MA, USA), the named CT2 method is based on the 3D Canny algorithm [31] and its methodology is
201 divided into four steps: (i) Preliminary surface detection, (ii) Sub-voxel resolution refinement, (iii)
202 Measurement and (iv) Measurement correction.

203 1. *Preliminary surface detection*
204 A Gaussian filter is applied along each of the three Cartesian directions, using a 1x10
205 convolution mask oriented along the direction. After this phase, three different 3D images (X–Y, Y–
206 Z and Z–X in Figure 5) are obtained, each showing the transition between materials along the
207 corresponding direction.

208 2. *Sub-voxel resolution refinement*
209 A specific algorithm has been operated to calculate the points with XYZ-coordinates that define,
210 with sub-voxel resolution, the material transition. This improves the actual spatial resolution of the
211 edge detection method down to one hundredth of the voxel resolution. From the preliminary surface
212 detected in the previous step, obtained from the calculated local maximum positions, a gravity
213 center algorithm is applied to a neighborhood around each of those local maximum positions. The
214 calculation of the optimal position of the point (X',Y',Z') inside it with sub-voxel resolution is carried
215 out by applying Eq.(1):

$$X' = \frac{\sum_{i=1}^{3}(X_i \cdot G_{X,i})}{\sum_{i=1}^{3}G_i}; \quad Y' = \frac{\sum_{j=1}^{3}(Y_j \cdot G_{Y,j})}{\sum_{j=1}^{3}G_j}; \quad Z' = \frac{\sum_{k=1}^{3}(Z_k \cdot G_{Z,k})}{\sum_{k=1}^{3}G_k} \tag{1}$$

216 being X_i, Y_j and Z_k the coordinates of the voxels inside the window, with i, j and k indicating the
217 number of voxel, i.e. from 1 to 3 for the optimal neighborhood size calculated for this work (see
218 Figure 5). $G_{X,i}$, $G_{Y,j}$ and $G_{Z,k}$, with possible values from 0 to 65,535 (i.e. 16 bits), are the gray value
219 transitions obtained in the preliminary surface detection phase for the X, Y and Z directions,
220 respectively. This refinement is carried out separately and independently along all the three XYZ
221 directions obtaining the three different coordinates of each surface point.
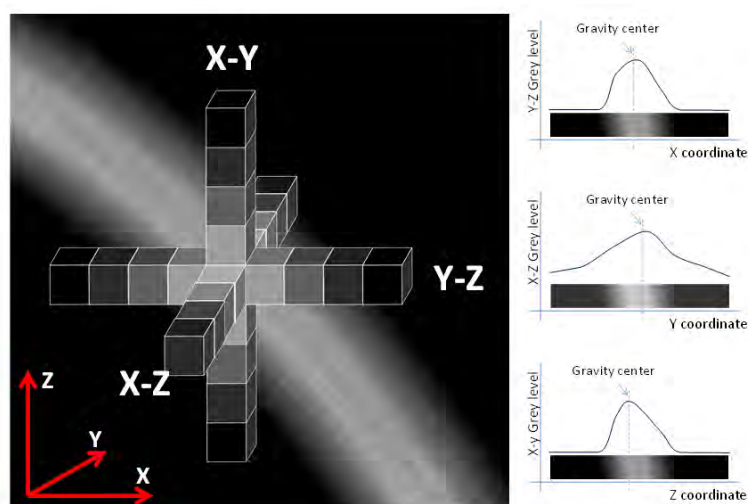
**Figure 5.** Sub-voxel resolution refinement (3D Canny algorithm, CT2).

3. Measurement

Using the point cloud of the part surface obtained from the previous step, coordinate measurements of the required dimensions can be carried out. This presents some challenges, especially for the 3D Canny algorithm since, as described above it uses an strategy that analyses the surface from the three main Cartesian directions in order to extract the point cloud. That was proven to be effective with regular surfaces than can be easily defined along those Cartesian axes [31]. However, in 3D complex geometries, which are not necessarily aligned with those Cartesian axes, the effectiveness of this algorithm is being analyzed in the present work.

4. Measurement correction

The correction applied in this work (Figure 6) includes the additional measurement of a specific parameter of the inspected part by another measuring technique (e.g. tactile or optical CMM). By comparing this result with the one obtained by the CT system a bias is calculated as a correction factor, which is applied to all the other measurements too. In the case presented the parameter used was again Dr (Figure 2) since it was simple to measure by a tactile CMM.

A more detailed explanation of the whole process can be found in [31].
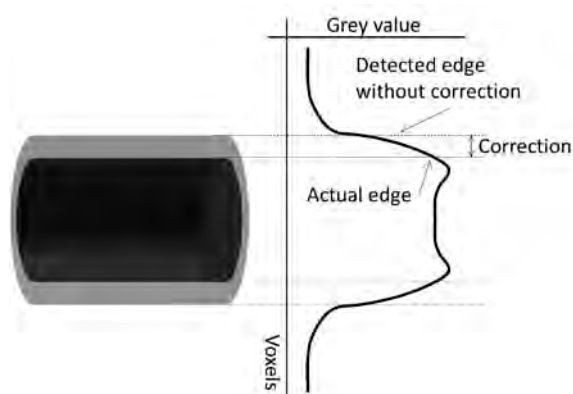
**Figure 6.** Measurement correction (3D Canny algorithm, CT2).

2.4. Optical coordinate measurements

Reference measurements of the endodontic file were performed on an optical coordinate measuring machine (OCMM) DeMeet 220 by Schut Geometrical Metrology (Groninge, The Netherlands) using a diascopic illumination with a light ring, a magnification lens 2x, an objective Numerical Aperture (NA) of 0.06 and a field of view of 3111 μm x 2327 μm. The uncertainty assessment of the OCMM measurements was carried out using a calibrated artefact. This artifact was

247 a glass-chromium mask scale with an expanded calibration uncertainty of ±0.5 µm (k=2). The
248 OCMM uncertainty for length measurements in the 100-1000 µm range was evaluated, resulting in
249 the maximum permissible error MPE$_{OCMM}$ = 1.7 µm (i.e. suitable for the diameter measurements of
250 the endodontic file). For the measurements of the endodontic file with a length L>1 mm, the
251 maximum permissible error of the OCMM obtained is: MPE$_{OCMM}$ = 5 µm + (L/150) µm (L in mm).

252 The 3D complex geometry of the dental file has been measured by the OCMM and the CT. Since
253 the OCMM is a 2D measuring system, the measurement repeatability has been evaluated,
254 considering different positions. A cube is firmly attached, using cyanoacrylate glue, to the workpiece
255 at the bottom of the cutting area of the file, in order to use their faces as reference for the coordinate
256 system (Figure 7a and Figure 10). Hence, the dental file measurement has been performed ten times
257 for each of the four orientations, each one determined by the face of the cube resting parallel to the
258 OCMM measuring stage (Figure 7b). Therefore, a direct comparison between the OCMM and the CT
259 measurements for each of the four orientations can be carried out.

(a)

(b)
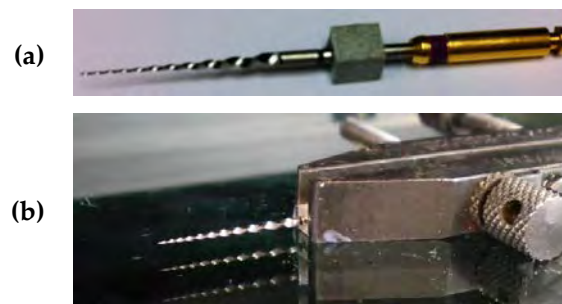
260 **Figure 7.** (**a**) Reference cube applied to the dental file; (**b**) dental file during the measurement on the
261 OCMM.

262 *2.5. Computed Tomography scanning*

263 The dental file was scanned using a General Electric eXplore Locus SP by GE Healthcare
264 (Chicago, IL, USA) cone-beam micro-CT machine. The reconstruction process was performed using
265 the software provided by the manufacturer. The selected parameters used for the CT measurements
266 were the presented in Table 1. During the scanning of the workpiece the temperature was
267 continuously recorded inside the machine, obtaining a temperature range of 20±2ºC. As shown in
268 Figure 8, a miniaturized ball-bar reference standard previously calibrated was also scanned with the
269 dental file. This reference allowed the determination of the scale factor and the correction of the scale
270 error of the measurements obtained.

271 **Table 1.** CT scanning parameters for the dental file workpiece.

Parameter	Value
Voltage	90 kV
Current	80 µA
Increment angle	0.4 degrees
Voxel size	28 µm

272

Miniaturized ball-bar
(scale factor correction)

19.911 mm ± 3 µm
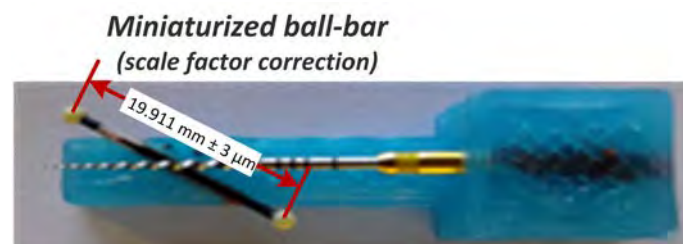
273

274 **Figure 8.** Dental file and miniaturized ball bar during the measurement on the CT scanner.

275   An example of the points cloud obtained after the surface extraction process can be observed in
276   Figure 9. Figure 9a shows the complete scan of the dental file (including the reference cube used for
277   the alignment of the measurement). In Figure 9b a detail of the dental file tip and of the 3D complex
278   helix geometry is presented. Measurements are performed over the point cloud in order to avoid
279   distortions caused by the surface reconstruction algorithms.
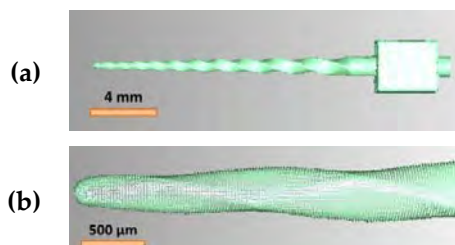
280   **Figure 9.** Point cloud from the CT scan of the file: (**a**) complete scan of the dental file; (**b**) detail of the
281   dental file tip and of the helix geometry.

282   *2.6. Measurement strategy*

283   A common measurement procedure and reference coordinate system to be used by both
284   measuring systems (i.e. OCMM and CT) was agreed. As it is introduced in subsection 2.4, it included
285   the use of a cube attached to the file in order to use their faces as reference for the coordinates system
286   (see Figure 7a). Since the OCMM is a 2D measuring system, the access to all surfaces to be measured
287   was achieved by placing the dental file in those four different orientations. The dental file
288   measurement by the CT scanner was reproduced using also the four cube faces orientations as
289   reference planes. As a consequence, a direct comparison between the OCMM 2D measurements and
290   the CT measurements results with the dental file in the same orientation could be performed in
291   terms of measurement repeatability.

292   The reference coordinate system for the dental file is obtained by a plane (one of the cube faces),
293   a straight line (the axial axis of the dental file) and a point as the origin of the XYZ-system. Firstly,
294   the XZ-plane is created taking the superior face of the cube (see Figure 10a). Secondly, the main long
295   Z-axis of the dental file is defined by joining the center of the spherical tip together with the center of
296   the base cylinder (see Figure 10b). The spherical tip of the file measured was 0.06 mm in diameter.
297   The cylinder is adjusted on the base of the endodontic file between the operative zone and the
298   reference cube at a distance of 0.2 mm from both elements, respectively. Finally, the origin is defined
299   as the intersection of the axial Z-axis and a plane measured on the cube face oriented to the dental
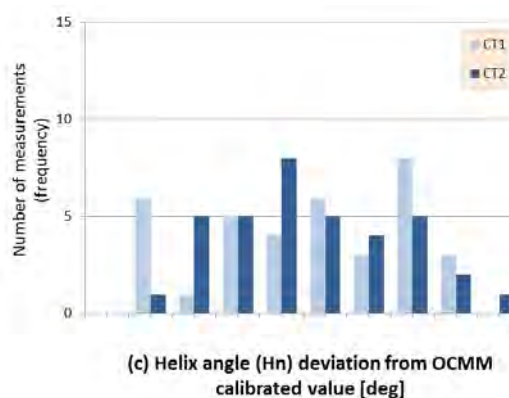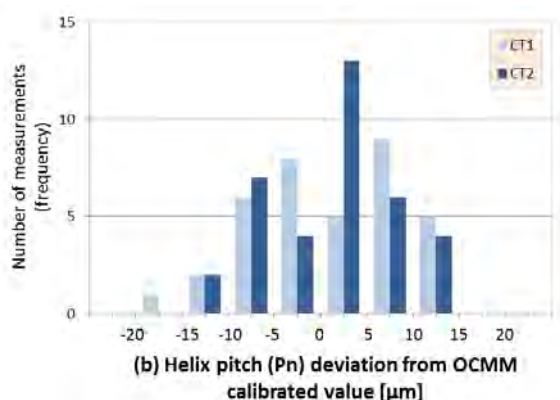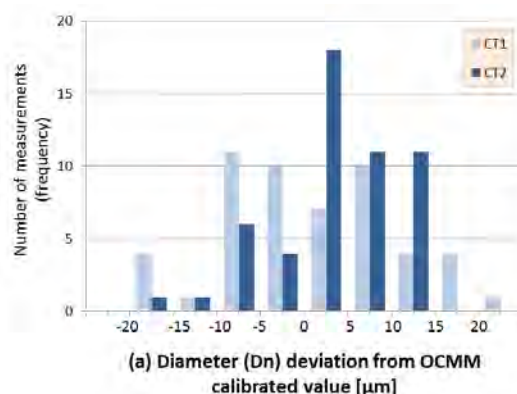300   file (see Figure 10c).
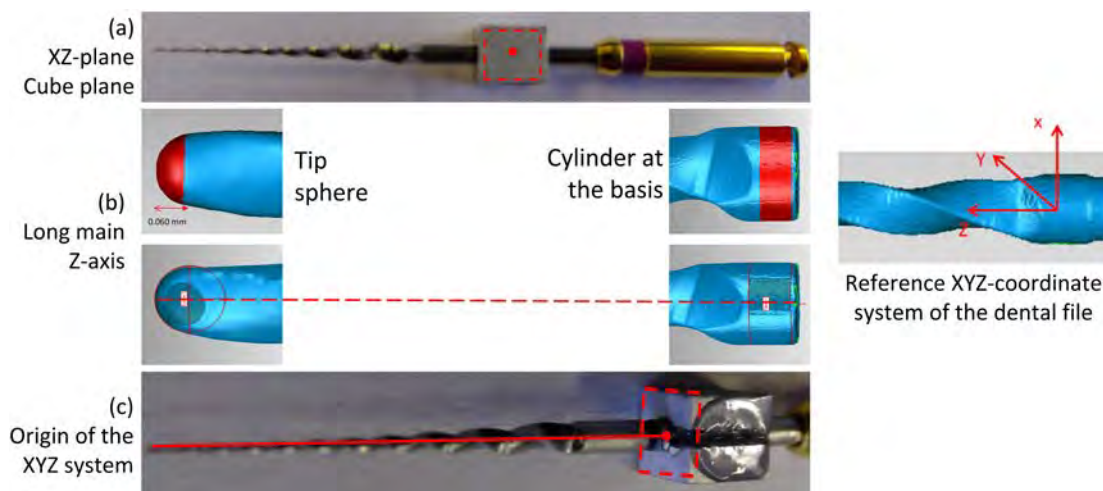
302   **Figure 10.** Measurement procedure of the dental file: (a) XZ-plane; (b) Z-axis; (c) XYZ-origin.

303 **3. Measurement results and uncertainty estimation**

304 *3.1. Systematic error analysis*

305 In order to compare the two surface extraction methods the first influence analyzed is the
306 systematic deviation of measurements by calculating the difference between the mean measurement
307 performed using the CT scanner and the reference value obtained by the OCMM. To provide a
308 comprehensive representation of all data for each type of measurand (diameters D_0 to D_{12}, helix
309 pitches P_1 to P_9 and helix angles H_1 to H_9) (see Figure 11) the distribution of the systematic error
310 results coming from the measurements taken at the four different orientations are used (one for
311 every face of the base cube). Figure 11 illustrates the number of measured error results (frequency is
312 indicated as bar heights, see Y axis) in each error interval considered (X axis). It can be observed that
313 the higher peaks (i.e. the higher number of measurement errors) tend to be centered in error
314 intervals close to zero, which indicates that the surface extraction methods used minimize bias
315 errors.

316 As it is shown in Figure 11a, Figure 11b and Figure 11c for diameter, helix pitch and helix angle
317 measurement results, respectively, the systematic errors are substantially influenced by the
318 employed surface extraction technique. In particular, the application of the CT2 technique (i.e. based
319 on 3D Canny) allows obtaining a higher number of measurements closer to the calibrated values
320 (higher bars close to zero) than when applying the CT1 technique (i.e. based on local threshold). On
321 the one hand, by applying the CT1 method, reference values for most of the elements to be measured
322 are usually needed in order to adjust the ISO factor [27], which could be particularly difficult when
323 measuring 3D complex geometries, as in the presented work. On the other hand, the edge detection
324 technique based on the Canny algorithm (CT2) provides a good edge location capability, less
325 dependent on the geometry of the measured part. It might be corrected by using only one
326 dimensional reference (Dr in this case). That significantly reduces the influence of the image quality,
327 i.e. image noise. Results from both methods are similar in the helix angle case (Figure 11c). This is
328 due to the fitting strategy for the determination of the tangent on the cutting edge and software
329 applied, which results more influent than the bias error.

(a) Diameter (Dn) deviation from OCMM
calibrated value [μm]

(b) Helix pitch (Pn) deviation from OCMM
calibrated value [μm]

(c) Helix angle (Hn) deviation from OCMM
calibrated value [deg]

330   **Figure 11.** Deviations distribution of (**a**) diameter, (**b**) helix pitch and (**c**) helix angle measurands,
331   obtained by CT system from OCMM calibrated values and applying CT1 and CT2 surface extraction
332   techniques.

333   *3.2. Uncertainty estimation for optical CMM measurements*

334   Optical CMM measurements were used to validate the CT measurements. The measurement
335   uncertainties for optical measurements with the OCMM were calculated according to ISO 14253-2
336   [38], considering two influence factors as described in equation (2):

$$U_{95,OCMM} = k\sqrt{u_{c,OCMM}^2 + u_{p,OCMM}^2} \tag{2}$$

337   where k is the coverage factor (k=2 for a coverage interval of 95.45%), $u_{c,OCMM}$ is the standard
338   uncertainty of the OCMM based on the MPE of this measuring system ($u_{c,OCMM}$=MPE$_{OCMM}$/2) and
339    $u_{p,OCMM}$ is the standard uncertainty of the measuring procedure, i.e. standard deviation of the
340   repeated measurements (repeatability, n=10). The OCMM is placed in a metrology laboratory with
341   standard conditions of temperature, 20±1°C and humidity, 50–70%.
342
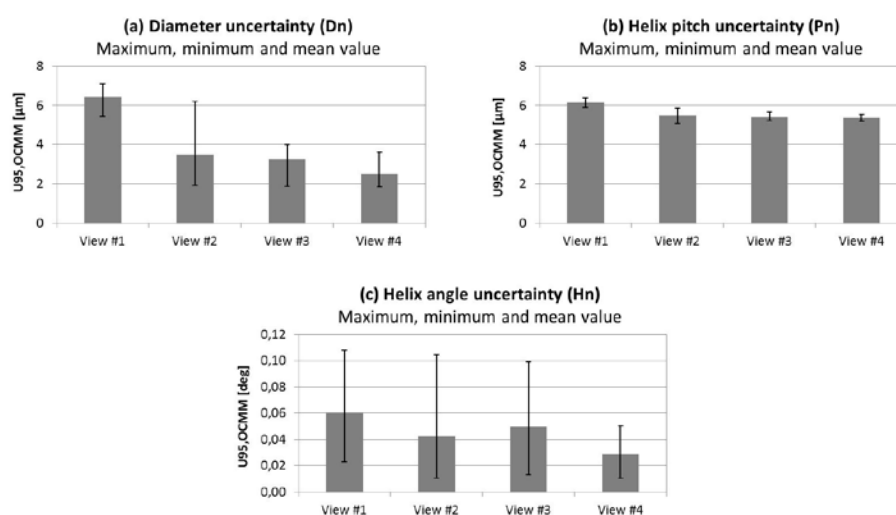
343   **Figure 12.** OCMM measurement uncertainty results of the four views and measurands (U$_{95,OCMM}$): (**a**)
344   Diameter, Dn; (**b**) Helix pitch, Pn; (**c**) Helix angle, Hn.

345   The results of the expanded uncertainty U$_{95,OCMM}$ were estimated for the four views and the four
346   selected measurands: length (La), variable diameter (Dn), helix pitch (Pn) and helix angle (Hn). The
347   angle measurement uncertainty was estimated by applying the error propagation law, as described
348   in the GUM [39]. The maximum, minimum and mean uncertainty values obtained for all the
349   parameters studied (Dn, Pn and Hn) are shown in Figure 12a, Figure 12b and Figure 12c,
350   respectively. As it is illustrated, those values can be assumed as representative for each measurand
351   of the whole workpiece. Thus, the maximum expanded uncertainty values from OCMM
352   measurements are:
353   • U$_{MAX,OCMM}$ (La) = 7.9 μm
354   • U$_{MAX,OCMM}$ (Dn) = 7.1 μm; (n=1,…,12)
355   • U$_{MAX,OCMM}$ (Pn) = 6.4 μm; (n=1,…,9)
356   • U$_{MAX,OCMM}$ (Hn) = 0.16 deg; (n=1,…,9)

357   *3.3. Uncertainty estimation for CT measurements*

358   Measurement uncertainties for CT system were calculated. Despite of the lack of accepted test
359   procedures and standards, numerous efforts have been focused on defining a fundamental

document for specification and verification of CT systems used for coordinate metrology. As a result, several VDI/VDE guidelines are nowadays the main basis for the future development of ISO standards. The main tests to evaluate length measurement and probing errors are specified in VDI/VDE 2630-1.3 [40]; and influencing factors and a guide for the determination of uncertainty are described in VDI/VDE 2630-2.1 [41], the most applied procedure and recent guideline of task-specific calibration based on the substitution method. In some cases, when the substitution method is not applicable because a previous calibration with a more accurate system is unfeasible (as it is in this case), the uncertainty estimation can be achieved according to ISO 14253-2 [38], by considering the main error contributors in CT, as shown in equation (3):

$$U_{95,CTi} = k\sqrt{u_r^2 + u_p^2 + u_w^2 + u_b^2} \tag{3}$$

The term k is the coverage factor (k=2) and the i-index (i=1,2) refers to the two surface extraction methods: CT1 (local threshold method) and CT2 (Canny algorithm) in order to obtain $U_{95,CT1}$ and $U_{95,CT2}$, respectively. The term u_r is the standard uncertainty due to traceability quantified by the MPE of the CT (u_r=MPE_{CTi}/2), which are respectively: MPE_{CT1} = 6.6 µm + (L/5.4) µm; and MPE_{CT2} = 7.0 µm + (L/5.6) µm, where L is in mm. These micro-CT system MPE expressions were experimentally determined by using several calibrated reference artefacts with maximum calibration uncertainties lower than ±3.0 µm for all the dimensions used. Additionally, u_P is the standard uncertainty of the measurement procedure (repeatability), u_w is the standard uncertainty from the material and manufacturing variations of the measured process, including the variations in the CTEs (coefficient of thermal expansion) of the workpiece, and u_b is the standard uncertainty associated with the residual systematic error of the measurement process, which is influenced by the surface extraction technique (mainly dependent on the measurement correction, so that the standard uncertainty of the scale factor and the applied offset determination are here considered) and by the influence of the temperature variation during the CT measuring process.
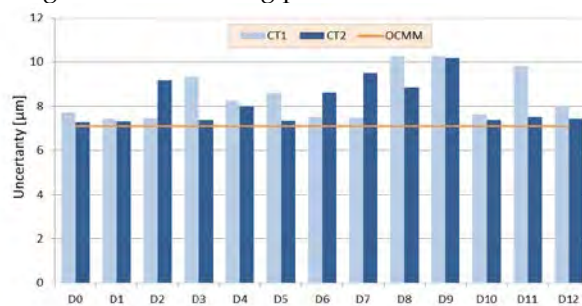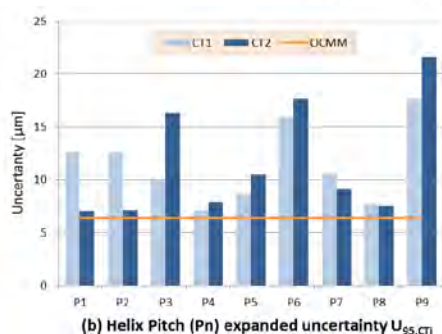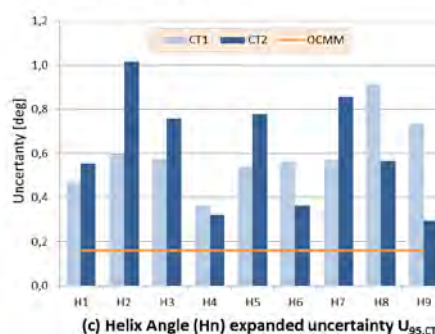
Figure 13. OCMM and CT expanded measurement uncertainty results (U_{95}) of the four views and measurands: (**a**) Diameter, Dn; (**b**) Helix pitch, Pn; (**c**) Helix angle (Hn).

The comparison between the expanded uncertainty $U_{95,CT1}$, $U_{95,CT2}$ and $U_{MAX,OCMM}$ is shown in Figure 13a, Figure 13b and Figure 13c for diameter, helix pitch and helix angle measurands, respectively. Considering the diameter, for smaller values of Dn the expanded uncertainty obtained by CT is closer than the considered $U_{MAX,OCMM}$. Since helix pitch and helix angle measurements

391 strongly depend on the fitting procedure from the point cloud, these measurands present higher
392 differences with respect to the reference OCMM value. If both surface extraction methods are
393 compared, there are not clear differences between them in most of the measurands. On the other
394 hand, in some cases CT1 shows lower uncertainties, while the opposite happens for some other
395 measurands. In addition, for a further analysis of these results, the estimated uncertainties are
396 eventually compared with the dental file's calibration and tolerances. Hence, in next subsection the
397 E_N value is calculated for all measurands and the 2U/T ratio is also estimated to compare both
398 extraction techniques when verifying 3D complex geometries in this micro manufactured part.

399 *3.4. E_N value and tolerance verification capability*

400 To validate the expanded uncertainty results in relation to the measuring uncertainty of the
401 used instruments, CT system and OCMM, the E_N value was calculated for all measurands [42]. This
402 parameter is given by equation (4) and relates the deviation between a measured value (i.e. by the
403 CT systems in the present case) and the corresponding calibrated value (i.e. by the CMS) concerning
404 their respective stated uncertainties. Then, if $E_N<1$ there is a satisfactory agreement between the two
405 values, otherwise there is no agreement among them.

$$E_N = \frac{|(CT_{meas.value}) - (OCMM_{ref.value})|}{\sqrt{U_{CT}^2 + U_{OCMM}^2}} \tag{4}$$

406 Figure 14 illustrates the percentage of $E_N<1$ values results for all the measurands of the dental
407 file. As in the previous subsection, not significant differences between both techniques are observed.
408 In general CT2 shows very similar or slightly better results, except for the measurand La or total
409 length of the cutting segment. Nevertheless, the represented percentage of this parameter only
410 considers that single parameter measured in the four orientations. For the rest of parameters more
411 measurands are considered (nine in four orientations for Helix Pitch, nine in four orientations for
412 Helix Angle, etc.). Again, this analysis cannot be considered conclusive in terms of defining which of
413 both techniques provides a lower measurement uncertainty.
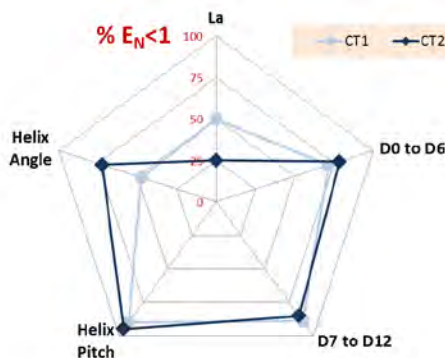
414

415 **Figure 14.** Percentage of $E_N<1$ values calculated for all CT measurement results and using both
416 surface extraction techniques (CT1, CT2).

417 The ratio 2U/T that considers the uncertainty measurement result (2U) and the tolerance of the
418 workpiece (T) was analyzed. To assure the measuring capability of the CT system and the applied
419 surface extraction techniques, the ratio must be 2U/T≤0.4, considering the micro-geometries of the
420 dental file [41,43]. As previously presented for the E_N value, the percentage of 2U/T≤0.4 values
421 results are represented in Figure 15. Nevertheless, the measurands considered are only the length of
422 the active cutting part (La) and variable diameters (D0 to D12), whose tolerance specifications were
423 defined. As it is shown, the 100% of OCMM measurements meet the requirement. Both surface
424 extraction methods CT1 and CT2 have also a high number of measurements that accomplish with
425 the tolerance ratio specification: 78.6% and 85.7%, respectively. The results provided for both
426 methods are similar. Nevertheless, CT2 or Canny algorithm offers a slightly better performance

427 according to the results shown in Figure 15. As a conclusion of the whole uncertainty assessment
428 study and despite higher uncertainties and challenges in performing CT scanning metrology, the use
429 of this technology for tolerance verification on complex geometries has been demonstrated to be
430 adequate.
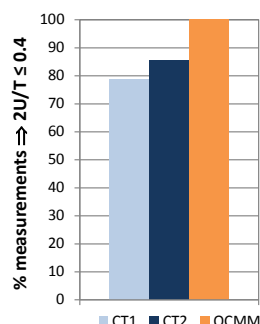
431

432 **Figure 15.** Percentage of 2U/T≤0.4 values calculated for all CT and OCMM measurement results with
433 tolerance specification and using both surface extraction techniques (CT1, CT2).

4. Conclusions

435 In this paper a comparative analysis of two surface extraction techniques in computed
436 tomography has been presented for the case study of a micro-component (a dental file) with 3D
437 complex geometry. The contribution of the post-processing phase in CT dimensional measurements
438 is here evaluated by applying the threshold determination strategy (CT1) and the Canny algorithm
439 (CT2). Reference measurements were performed on an optical coordinate measuring machine
440 (OCMM). Considering systematic errors results, it was found that the edge detection technique CT2
441 provides an edge definition with slightly lower systematic errors and, therefore, less dependent on
442 the geometry of the measured part. Furthermore, the 3D Canny adapted method includes a direct
443 correction instead of the iterative correction method of the local threshold, which simplifies its
444 application. The uncertainty results do not show a clear difference between both techniques,
445 although slightly better results have been observed for CT2 than for CT1, especially when the
446 tolerance verification has been analyzed. Therefore, from this study both the threshold
447 determination strategy and the 3D Canny technique show a similar behavior when tolerance is
448 verified by performing CT scanning metrology on complex micro-geometries.
449 Consequently, regarding the 3D Canny algorithm it can be concluded that concerning accuracy
450 and uncertainty it is, at least, as effective as the threshold technique when it is used for 3D complex
451 micro-geometry dimensional measurements. This confirms the results obtained in [31] for regular
452 and more simple geometries.
453 Particularly, since the 3D Canny adapted method includes a direct correction instead of the
454 iterative correction method of the local threshold, its impact lies on the fact that once the point
455 cloud generated by the CT system is calibrated with relatively low uncertainty, all the points of the
456 cloud will be constrained in a position which is also determined with a relatively low systematic
457 error (slightly lower with the Canny method than by using a thresholding technique) and
458 uncertainty (similar with both techniques). Potentially, such calibration will be applicable and valid
459 as well as to any relative position between different points of the cloud, leading to the result that
460 virtually any measurement of complex and/or freeform geometrical features can be also performed
461 with relatively low uncertainty. The metrological verification of this possibility is dependent on the
462 availability of a calibrated freeform surface. On this regards, challenges are still present in the
463 procedure for some complex measurands of the dental file such as the helix angle, and for
464 geometrical characteristics with a critical measurand definition such as the length of the active
465 cutting edge. Further research work will be focused on the establishment of a traceable and
466 reproducible procedure for the calibration of miniaturized high accuracy freeform components in
467 order to obtain a three-dimensional uncertainty assessment of CT measurements.

References

1. Tosello, G.; Hansen, H. N.; Gasparin, S. Applications of dimensional micro metrology to the product and process quality control in manufacturing of precision polymer micro components. *CIRP Ann. - Manuf. Technol.* **2009**, *58*, 467–472.

2. Bos, E. J. C. Aspects of tactile probing on the micro scale. *Precis. Eng.* **2011**, *35*, 228–240.

3. Petz, M.; Tutsch, R.; Christoph, R.; Andraes, M.; Hopp, B. Tactile–optical probes for three-dimensional microparts. *Measurement* **2012**, *45*, 2288–2298.

4. Claverley, J. D.; Leach, R. K. A review of the existing performance verification infrastructure for micro-CMMs. *Precis. Eng.* **2015**, *39*, 1–15.

5. Mathia, T. G.; Pawlus, P.; Wieczorowski, M. Recent trends in surface metrology. *Wear* **2011**, *271*, 494–508.

6. Bešić, I.; Van Gestel, N.; Kruth, J.-P.; Bleys, P.; Hodolič, J. Accuracy improvement of laser line scanning for feature measurements on CMM. *Opt. Lasers Eng.* **2011**, *49*, 1274–1280.

7. De Chiffre, L.; Carmignato, S.; Kruth, J.-P.; Schmitt, R.; Weckenmann, A. Industrial applications of computed tomography. *CIRP Ann. - Manuf. Technol.* **2014**, *63*, 655–677.

8. Yu, J.; Lynn, R.; Tucker, T.; Saldana, C.; Kurfess, T. Model-free subtractive manufacturing from computed tomography data. *Manuf. Lett.* **2017**, *13*, 44–47.

9. Hermanek, P.; Carmignato, S. Porosity measurements by X-ray computed tomography: Accuracy evaluation using a calibrated object. *Precis. Eng.* **2017**, *49*, 377–387.

10. Villarraga-Gómez, H.; Lee, C.; Smith, S. T. Dimensional metrology with X-ray CT: A comparison with CMM measurements on internal features and compliant structures. *Precis. Eng.* **2018**, *51*, 291–307.

11. Heinzl, C.; Kastner, J.; Gröller, E. Surface extraction from multi-material components for metrology using dual energy CT. *IEEE Trans. Vis. Comput. Graph.* **2007**, *13*, 1520–1527.

12. Krämer, P.; Weckenmann, A. Multi-energy image stack fusion in computed tomography. *Meas. Sci. Technol.* **2010**, *21*, 45105.

13. Borges de Oliveira, F.; Stolfi, A.; Bartscher, M.; De Chiffre, L.; Neuschaefer-Rube, U. Experimental investigation of surface determination process on multi-material components for dimensional computed tomography. *Case Stud. Nondestruct. Test. Eval.* **2016**, *6*, 93–103.

14. Kiekens, K.; Welkenhuyzen, F.; Tan, Y.; Bleys, P.; Voet, A.; Kruth, J.-P.; Dewulf, W. A test object with parallel grooves for calibration and accuracy assessment of industrial computed tomography (CT) metrology. *Meas. Sci. Technol.* **2011**, *22*, 115502.

15. Xue, L.; Suzuki, H.; Ohtake, Y.; Fujimoto, H.; Abe, M.; Sato, O.; Takatsuji, T. A method for improving measurement accuracy of cylinders in dimensional CT metrology. *Comput. Des.* **2015**, *69*, 25–34.

16. Stolfi, A.; De Chiffre, L. 3D artefact for concurrent scale calibration in Computed Tomography. *CIRP Ann. - Manuf. Technol.* **2016**, *65*, 499–502.

17. Andreu, V.; Georgi, B.; Lettenbauer, H.; Yague, J. A. Analysis of the error sources of a Computer Tomography Machine. In *Proc. Lamdamap conference*; 2009; pp. 462–471.

18. Kruth, J. P.; Bartscher, M.; Carmignato, S.; Schmitt, R.; De Chiffre, L.; Weckenmann, A. Computed

512 tomography for dimensional metrology. *CIRP Ann. - Manuf. Technol.* **2011**, *60*, 821–842.

513 19. Hiller, J.; Reindl, L. M. A computer simulation platform for the estimation of measurement uncertainties in

514 dimensional X-ray computed tomography. *Meas. J. Int. Meas. Confed.* **2012**, *45*, 2166–2182.

515 20. Weckenmann, A.; Krämer, P. Assessment of measurement uncertainty caused in the preparation of

516 measurements using computed tomography. In *19th IMEKO World Congress 2009*; Quality Management and

517 Manufacturing Metrology, University Erlangen-Nuremberg, Erlangen, Germany, 2009; Vol. 3, pp. 1787–1791.

518 21. Ferrucci, M.; Ametova, E.; Carmignato, S.; Dewulf, W. Evaluating the effects of detector angular

519 misalignments on simulated computed tomography data. *Precis. Eng.* **2016**, *45*, 230–241.

520 22. Hiller, J.; Reindl, L. M. A computer simulation platform for the estimation of measurement uncertainties in

521 dimensional X-ray computed tomography. *Measurement* **2012**, *45*, 2166–2182.

522 23. Ferrucci, M.; Leach, R. K.; Giusca, C.; Carmignato, S.; Dewulf, W. Towards geometrical calibration of x-ray

523 computed tomography systems—a review. *Meas. Sci. Technol.* **2015**, *26*, 92003.

524 24. Müller, P.; Cantatore, A.; Andreasen, J. L.; Hiller, J.; De Chiffre, L. Computed tomography as a tool for

525 tolerance verification of industrial parts. In *Procedia CIRP*; 2013; Vol. 10, pp. 125–132.

526 25. Müller, P.; Hiller, J.; Cantatore, A.; De Chiffre, L. A study on evaluation strategies in dimensional X-ray

527 computed tomography by estimation of measurement uncertainties. *Int. J. Metrol. Qual. Eng.* **2012**, *3*, 107–115.

528 26. Stolfi, A.; Thompson, M. K.; Carli, L.; De Chiffre, L. Quantifying the Contribution of Post-Processing in

529 Computed Tomography Measurement Uncertainty. *Procedia CIRP* **2016**, *43*, 297–302.

530 27. Hiller, J.; Hornberger, P. Measurement accuracy in X-ray computed tomography metrology: Toward a

531 systematic analysis of interference effects in tomographic imaging. *Precis. Eng.* **2016**, *45*, 18–32.

532 28. Kraemer, A.; Lanza, G. Assessment of the Measurement Procedure for Dimensional Metrology with X-ray

533 Computed Tomography. *Procedia CIRP* **2016**, *43*, 362–367.

534 29. Ontiveros, S.; Yagüe-Fabra, J. A.; Jiménez, R.; Tosello, G.; Gasparin, S.; Pierobon, A.; Carmignato, S.; Hansen,

535 H. N. Dimensional measurement of micro-moulded parts by computed tomography. *Meas. Sci. Technol.* **2012**,

536 *23*, 125401.

537 30. Jiménez, R.; Ontiveros, S.; Carmignato, S.; Yagüe-Fabra, J. A. Fundamental correction strategies for accuracy

538 improvement of dimensional measurements obtained from a conventional micro-CT cone beam machine. *CIRP*

539 *J. Manuf. Sci. Technol.* **2013**, *6*, 143–148.

540 31. Yagüe-Fabra, J. A.; Ontiveros, S.; Jiménez, R.; Chitchian, S.; Tosello, G.; Carmignato, S. A 3D edge detection

541 technique for surface extraction in computed tomography for dimensional metrology applications. *CIRP Ann. -*

542 *Manuf. Technol.* **2013**, *62*, 531–534.

543 32. Ontiveros, S.; Yagüe, J. A.; Jiménez, R.; Brosed, F. Computed Tomography 3D Edge Detection Comparative

544 for Metrology Applications. *Procedia Eng.* **2013**, *63*, 710–719.

545 33. Ruddle, C. J. The ProTaper endodontic system: geometries, features, and guidelines for use. *Dent. Today*

546 **2001**, *20*, 60–67.

547 34. Ruddle, C. J. The ProTaper technique. *Endod. Top.* **2005**, *10*, 187.

548 35. ISO 3630-1:2008. Dentistry. Root-canal instruments. Part 1: General requirements and test methods 2008.

549 36. Stolfi, A.; Thompson, M. K.; Carli, L.; De Chiffre, L. Quantifying the Contribution of Post-Processing in

550 Computed Tomography Measurement Uncertainty. *Procedia CIRP* **2016**, *43*, 297–302.

551 37. Kiekens, K.; Welkenhuyzen, F.; Tan, Y.; Bleys, P.; Voet, A.; Kruth, J.-P. A test object for calibration and

552 accuracy assessment in X-ray CT metrology. *Proc. IMEKO 10th Int. Symp. Meas. Qual. Control* **2010**, *B6_86_1-4.*

553 38. ISO 14253-2:2011. Geometrical product specifications (GPS). Inspection by measurement of workpieces and

554 measuring equipment. Part 2: Guidance for the estimation of uncertainty in GPS measurement, in calibration of

555 measuring equipment and in product verifi 2011.

556 39. Guide to the Expression of Uncertainty in Measurement (GUM) 2008.

557 40. VDI/VDE 2630 Part 1.3 Guideline for the application of DIN EN ISO 10360 for coordinate measuring

558 machines with CT-sensors 2011.

559 41. VDI/VDE 2630 Part 2.1 Determination of the uncertainty of measurement and the test process suitability of

560 coordinate measurement systems with CT sensors 2015.

561 42. ISO/IEC 17043. Conformity assessment. General requirements for proficiency testing 2010.

562 43. ISO 286-2:2010. Geometrical product specifications (GPS). ISO code system for tolerances on linear sizes.

563 Part 2: Tables of standard tolerance classes and limit deviations for holes and shafts 2010.

564